Swarm Satellite Observations of the Effect of Prompt Penetration Electric Fields (PPEFs) on Plasma Density around Noon and Midnight Side of Low Latitudes during the 07–08 September…

Article *in* Advances in Space Research · November 2021

DOI: 10.1016/j.asr.2021.11.027

CITATIONS
2

READS
65

1 author:

Erdinç Timoçin
Mersin University
18 PUBLICATIONS **70** CITATIONS

SEE PROFILE

Available online at www.sciencedirect.com

ScienceDirect

Advances in Space Research 69 (2022) 1335–1343

ADVANCES IN SPACE RESEARCH (a COSPAR publication)

www.elsevier.com/locate/asr

Swarm satellite observations of the effect of prompt penetration electric fields (PPEFs) on plasma density around noon and midnight side of low latitudes during the 07–08 september 2017 geomagnetic storm

Erdinç Timoçin

Vocational School of Technical Sciences, Department of Medical Services and Techniques, Mersin University, 33334 Mersin, Turkey

Received 29 June 2021; received in revised form 20 November 2021; accepted 24 November 2021
Available online 30 November 2021

Abstract

In this paper, using plasma density data (N_e) obtained from the Swarm satellite, the effect of prompt penetration electric fields (PPEFs) on the distribution of plasma density at low latitudes during the 07–08 September 2017 geomagnetic storm is discussed. The observations of enhancements and reductions in ionospheric plasma around noon and midnight in association with the orientation of the north–south component of the interplanetary magnetic field (IMF B_z) are presented during the main phase and the recovery phase of geomagnetic storm. The days of 05–06 September 2017 were selected as geomagnetically quiet days, and the plasma density data on these days were plotted as a quiet-time reference. The plasma enhancements and reductions in the low latitudes are found closely related to the magnetic local time (MLT), the orientation of IMF B_z, the main phase and the recovery phase of geomagnetic storm. During the main phase of geomagnetic storm with southward IMF B_z, plasma density increased around noon (10:00–11:00 MLT), while plasma density decreased around midnight (22:00–23:00 MLT). During the recovery phase of geomagnetic storm with northward IMF B_z, plasma density decreased around noon (10:00–11:00 MLT), while plasma density increased around midnight (22:00–23:00 MLT). The plasma density around both noon and midnight after the geomagnetic storm shows a distribution very similar to the distribution of plasma density during the geomagnetically quiet period. It is assumed that PPEFs are responsible for these results. During the main phase of the geomagnetic storm, the eastward PPEFs cause an increase in plasma density around the noon side while the westward PPEFs cause a decrease in plasma density around midnight side.

Keywords: Low latitudes; Swarm satellite; Plasma density data; Geomagnetic storms; Prompt penetration electric fields (PPEFs)

1. Introduction

It is known that the ionospheric plasma density in the equatorial, low, middle and high latitude regions is changed by different physical and chemical processes that are related to each other (Kivelson and Russell, 1995; Prölss, 2004; Tascione, 2010). The distribution of ionospheric plasma density in the equatorial and low latitude regions is controlled by electrodynamics processes in the E and F regions, which vary due to changes in geomagnetic activity. The primary reason for the plasma density variations in low latitudes during geomagnetically quiet periods is the low latitude electric field produced by the neutral wind dynamo. This electric field is in the eastward direction on the dayside, while it is in westward direction on the nightside. This electric field cause electrons over the equatorial and low latitude regions E × B drift which is upward dur-

E-mail address: erdinctimocin@mersin.edu.tr

https://doi.org/10.1016/j.asr.2021.11.027
0273-1177/

ing daytime and downward in nighttime. (Schunk and Nagy, 2000; Danilov and Laštovička, 2001; Prölss, 2004; Gilda de Lourdes, 2021).

During geomagnetically active periods, the plasma density at the equatorial and low latitudes is drastically modified by two main electrodynamics processes. The first process is prompt penetration electric fields (PPEFs), and the second process is disturbance dynamo electric fields (DDEFs). Different orientation of IMF B_z and different phases of geomagnetic storm occur different PPEFs, which causes different distributions at ionospheric plasma density. Since it was focused on the effects of PPEFs on the low latitude ionosphere in this study, the mechanism of PPEFs is only mentioned (Schunk and Nagy, 2000; Danilov and Laštovička, 2001; Prölss, 2004; Veenadhari et al., 2010; Yong et al., 2015; Veenadhari et al., 2019; Kumiko et al., 2020).

Atsuhiro (1968) proposed the PPEFs for the first time. Jaggi and Wolf (1973) made the theoretical explanation of this phenomenon that was so-called the shielding mechanism. The source of the shielding electric fields and PPEFs are the polarized electric field in the ring current region and the convection electric field in the outer magnetosphere, respectively. Region 1 (R1) field aligned current (FAC) in the polar cap associated with the convection electric field in the outer magnetosphere is called the prompt penetration electric field, while Region 2 (R2) field aligned current (FAC) in the polar cap associated with the polarized electric field in the ring current region is called the shielding electric field. The directions of these electric fields are opposite, and two processes, called undershielding and overshielding occur according to their equilibrium status. In the undershielding event, the convection electric field is larger than the shielding electric field, while in the overshielding event, the shielding electric field is greater than the convection electric field (Takashi et al., 2008; Yong et al., 2015). The southward turning of the IMF B_z causes the R1 FAC to increase rapidly. But the increase in R2 FAC takes a long time because it depends on the development of the shielding electric field in relation to the polarization process in the ring current region. Thus, the convection electric field in the outer magnetosphere penetrates into the equatorial and low latitude regions and this process is as called the undershielding phenomenon. The undershielding usually occurs during the main phase of the geomagnetic storm. During undershieilding conditions, PPEFs are eastward on the dayside, while they are westward on the nightside. The eastward PPEFs on the dayside cause the upward $E \times B$ drift of electrons over the equatorial and low latitude regions which turns out positive ionospheric storms in the dayside, while the westward PPEFs on the nightside cause the downward $E \times B$ drift of electrons over the equatorial and low latitude regions which turns out negative ionospheric storms in the nightside (Chao and John, 2005; Huba et al., 2005; Chao et al., 2007; Libo et al., 2008; Takashi et al., 2008; Tsurutani et al., 2008; Dashora et al., 2009; Veenadhari et al., 2010; Guo et al., 2011; Yosuke and Michael, 2015; Yong et al., 2015).

The northward turning of the IMF B_z causes the R2 FAC to increase strongly. Thus, the shielding electric field penetrates into the equatorial and low latitude regions and this process is as called the overshielding. The overshielding usually occurs during the recovery phase of the geomagnetic storm. During overshieilding conditions, PPEFs are westward on the dayside, while they are eastward on the nightside. The westward PPEFs on the dayside cause the downward $E \times B$ drift of electrons over the equatorial and low latitude regions which turns out negative ionospheric storms in the dayside, while the eastward PPEFs on the nightside cause the upward $E \times B$ drift of electrons over the equatorial and low latitude regions which turns out positive ionospheric storms in the nightside (Astafyeva et al., 2018; Erdinç, 2019a, 2019b; Veenadhari et al., 2019; Akala et al., 2020; Kumiko et al., 2020; Arowolo, et al., 2021).

Important attempts have been made to understand the effects of PPEFs on ionospheric and magnetospheric parameters at the equatorial, low and middle latitudes (Chao and John, 2005; Huba et al., 2005; Chao et al., 2007; Libo et al., 2008; Takashi et al., 2008; Tsurutani et al., 2008; Dashora et al., 2009; Veenadhari et al., 2010; Guo et al., 2011; Yosuke and Michael, 2015; Yong et al., 2015; Astafyeva et al., 2018; Erdinç, 2019a, 2019b; Veenadhari et al., 2019; Akala et al., 2020; Kumiko et al., 2020; Younas, et al., 2020; Arowolo, et al., 2021). In these studies, data sets such as Total Electron Content (TEC), electron density, ionospheric critical frequency (foF2), geomagnetic field and electric field derived from different instruments such as GPS, satellite, incoherent scatter radar, ionosonde, and magnetometer were used for different local time and longitudinal regions. The studies indicated that ionospheric electric field increases over mid and low latitudes during the main phase of the geomagnetic storm and these increases are related to the level of geomagnetic activity. The drift velocity in the equatorial F region increases during the daytime, while it decreases during the nighttime. The total electron content (TEC) in the daytime on the low latitude region increased by up to a factor of two. During the main phases of geomagnetic storms, the foF2 values at low latitude increase on dayside, while the foF2 values decrease on nightside. However, during the recovery phases of geomagnetic storms, the foF2 values decrease at dayside, while the foF2 values increase on nightside. The interplanetary electric field (IEF) penetrates to low latitude during geomagnetic storms and its orientation is closely related to the orientation of IMF B_z (Yong et al., 2015; Astafyeva et al., 2018; Veenadhari et al., 2019; Kumiko et al., 2020).

In this paper, the effect of prompt penetration electric fields (PPEFs) on the plasma density obtained from the SWARM satellite around noon and midnight of low latitudes was examined during the 07–08 September 2017 geomagnetic storm.

2. Materials and method of analysis

The main focus of this paper is to investigate effects of the Prompt Penetration Electric Fields (PPEFs) on the distributions of plasma density in low latitudes under overshielding and undershielding conditions of the 07–08 September 2017 geomagnetic storm. It specifically was focused on around noon and midnight sectors in order to clearly examine the effects of PPEFs on low latitude ionosphere around the noon and midnight. For this study, plasma density data from European Space Agency (ESA) Swarm satellite for low latitudes during 05–10 September 2017 is used when the satellite was in orbit around local noon (10:00–11:00 MLT) and around local midnight (22:00–23:00 MLT). Swarm is the mission of the ESA to explore the Earth's magnetic field, upper atmosphere, and ionosphere. It provides hourly, 1 min and 1 s high-resolution measurement of magnetic and electric fields, plasma density, electron and ion temperatures. The Swarm satellites consists of three satellites (Alpha, Bravo, and Charlie) placed on near-polar (87.5° and 88° inclination) orbits and move with a period by about 1.5 h. In this study, 1 s resolution plasma density data measured by Swarm Alpha in the ionospheric region between 441 km and 454 km altitude is used. Data was obtained via the VirES for Swarm (https://vires.services/).

The days of 05–06 September 2017 were selected as geomagnetically quiet days, and the plasma density data on these days were plotted as a quiet-time reference. For geomagnetic quiet days, the global geomagnetic activity index (K_p) is less than or equal to 3. Thus, the change of the plasma density around noon and midnight of low-latitude in response to the reorientations of IMF B_z and different phases of geomagnetic storm was compared with the values over the quiet days. Firstly, variation of plasma density around the noon and midnight side between 20:00 UT and 06:00 UT on 07 and 08 September 2017 was plotted, so that it can be possible to investigate the effect of PPEFs on the plasma density around the noon and midnight side during the main phase of the geomagnetic storm with southward IMF B_z and the recovery phase of geomagnetic storm with northward IMF B_z. Next, it was plotted temporal variation of IMF B_z, Dst and plasma density around midnight side and around noon side in groups of two days between 05 and 10 September 2017, so that it can be possible to compare the distribution of plasma density for geomagnetically active and quiet days.

3. Results and discussion

Fig. 1 (a-d) show temporal variation of IMF B_z and Dst, latitudinal variation of the plasma density (N_e) measured by the Swarm satellite around noon (~10:30 MLT) and midnight (~22:30 MLT) from 20:00 UT to 06:00 UT on 07 and 08 September 2017, respectively. The cases of Fig. 1a and b can be divided into two intervals. For Fig. 1a, the first interval is 4 h with southward IMF B_z from 21:00 UT to 00:00 UT, while the second interval is 5 h with northward IMF B_z from 01:00 UT to 05:00 UT. Note that the northward turning of IMF B_z also includes significant decrease in the magnitude of southward IMF B_z (still remains southward for 01:00 UT). For Fig. 1b, the first interval (as called main phase of geomagnetic storm) is 5 h between 21:00 and 01:00 when Dst values decrease. The minimum value of Dst during this time interval is −124 nT. The second interval (as called recovery phase of geomagnetic storm) is 5 h between 02:00 and 06:00 when Dst values increase. Because the IMF B_z and Dst values at 20:00 UT on 07 September was close to the geomagnetically quiet value (around 0), the plasma density data of noon (~10:30 MLT) and midnight (~22:30 MLT) for this hour are selected as a quiet-time data. For the case of Fig. 1a, the IMF B_z starts to southward turning at 21:00 UT, increase gradually in magnitude, and reaches its maximum value with −24 nT at 00:00 UT. Although IMF B_z still remains southward for 01:00 UT, the IMF B_z starts to northward turning at 01:00 UT, increase gradually in magnitude, and reaches its maximum value with 11 nT at 05:00 UT. Then IMF B_z become close to the geomagnetically quiet value at 06:00 UT. It can be seen from Fig. 1b that Dst value starts to decrease gradually from 21:00 UT and reaches its minimum value with −124 nT at 01:00 UT. The main phase of the geomagnetic storm ends at 01:00 UT. Then the recovery phase of the geomagnetic storm starts and Dst value increases gradually from 01:00 UT. The IMF B_z is southward during the main phase of geomagnetic storm, while it is usually northward during the recovery phase of geomagnetic storm.

The plasma density data around noon (~10:30 MLT) and midnight (~22:30 MLT) for 20:00 UT was plotted as quiet-time reference data (top graphic of Fig. 1c and d). The Swarm satellite data around noon (Fig. 1c) were not available for 22:00 UT on 07 September and for 01:00 UT, 04:00 UT and 06:00 UT on 08 September, while the Swarm satellite data around midnight (Fig. 1d) were not available for 21:00 UT on 07 September and for 00:00 UT, 02:00 UT and 05:00 UT on 08 September. The 4-hour continuous enhancement in the magnitude of southward IMF B_z during the main phase of the geomagnetic storm increased gradually the plasma density around noon between 21:00 UT and 00:00 UT. The enhancement in plasma density occurred almost immediately after IMF southward turning at 21:00 UT. When the magnitude of the southward IMF B_z has its maximum at 00:00 UT, the plasma density reached its maximum values for around noon. The plasma density around noon has two peak values around 6°S and 23°N latitudes. The plasma density around these latitudes was increased by a factor of 5–6 compared to the previous quiet-time values. However, the plasma density around midnight showed a decrease gradually in response to the southward turning of IMF B_z between 21:00 UT and 00:00 UT.

The plasma density around noon showed a sudden decrease in response to the IMF northward turning at

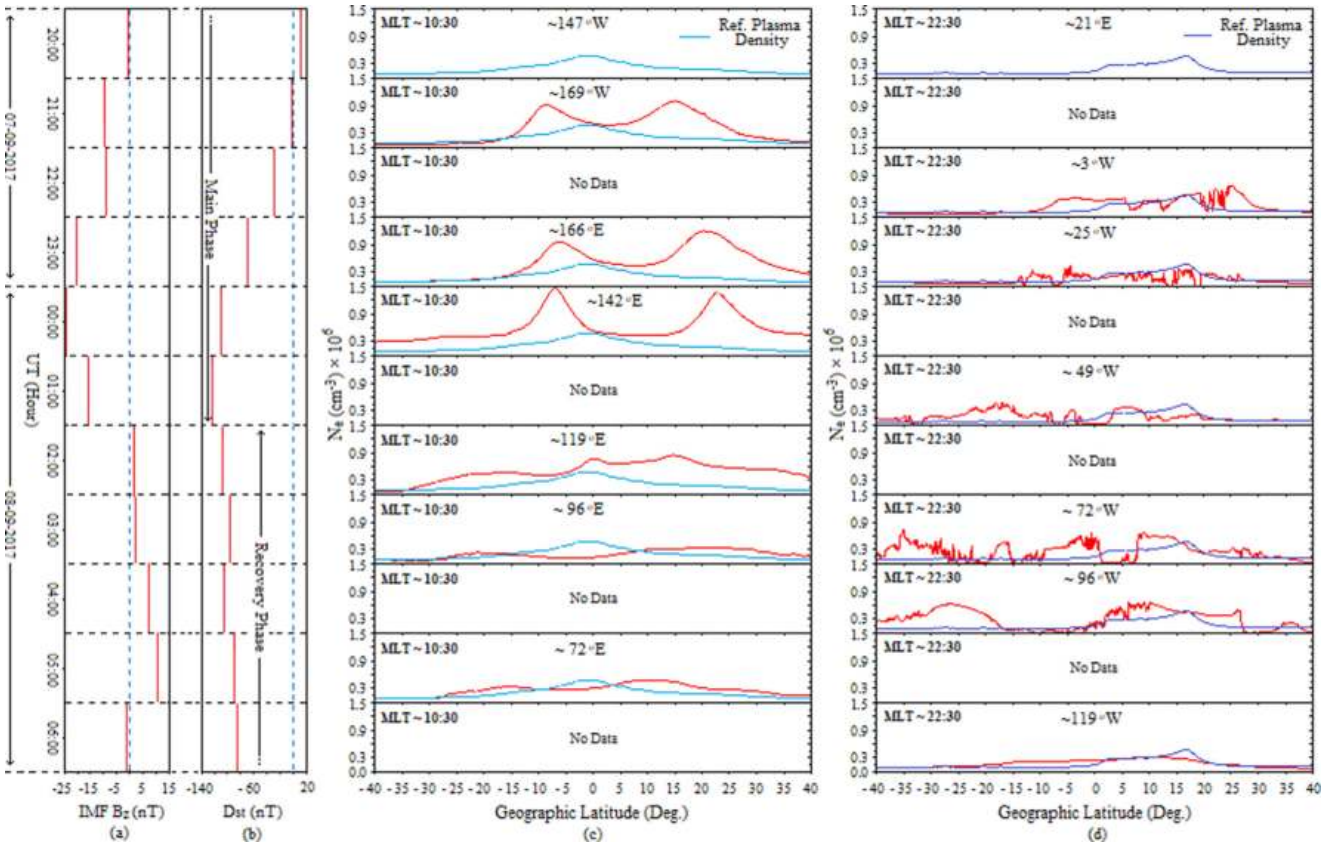

Fig. 1. Between 20:00 UT and 06:00 UT on 07–08 September 2017 (a) Variation of IMF B_z. (b) Variation of Dst. (c) Latitudinal variation of plasma density (N_e) around noon (~10:30 MLT). (d) Latitudinal variation of plasma density (N_e) around midnight (~22:30 MLT).

02:00 UT. This decrease in plasma density occurred at a maximum level between 5°S and 15°S latitudes and between 20°N and 30°N latitudes. The decrease in plasma density continued with the increase in the magnitude of the northward IMF B_z. The plasma density around 6°S and 23°N latitudes for 03:00 UT was decreased by a factor of 10 and 5 compared to the plasma density around 6°S and 23°N latitudes for 00:00 UT. However, the 4-hour continuous enhancement in the magnitude of northward IMF B_z during the recovery phase of the geomagnetic storm increased gradually the plasma density around midnight between 01:00 UT and 04:00 UT. The plasma density around midnight at 06:00 UT was close to the quiet-time data at 20:00 UT.

Fig. 2a and b show the temporal variation of IMF B_z and Dst during 05–06 September 2017, respectively. The blue dashed line indicates the geomagnetic quiet value. It can be seen from Fig. 2a and b that IMF B_z and Dst values have around geomagnetically quiet value during this period. Therefore, 05–06 September 2017 period was selected as geomagnetically quiet-time. Fig. 2c and d show the temporal variation of plasma density (N_e) as a function of geographic latitude and longitude around noon (10:00–11:00 MLT) and the temporal variation of plasma density (N_e) as a function of geographic latitude and longitude around midnight (22:00–23:00 MLT) during 05–06 September 2017, respectively.

For the eastern longitudes of Fig. 2c, the plasma density has the highest values between 10°S and 20°N. Between 01:00 and 07:00 UT on September 05, the plasma density has two peak values around 5°S and 15°N. For latitudes outside region between 10°S and 20°N, the plasma density gradually decreases as the latitude increases in both hemispheres. For the western longitudes of Fig. 2c, plasma density has maximum values during South Atlantic Anomaly region between 15°N and 25°S. For latitudes outside this region, the plasma density gradually decreases as the latitude increases in both hemispheres. For the eastern longitudes of Fig. 2d, although regional increases in plasma density were observed between 10°N and 10°S, it usually has values less than 0.3×10^6 cm^{-3}. For the western longitudes of Fig. 2d, the plasma density generally shows a distribution with values less than 0.45×10^6 cm^{-3} outside the region bounded by 5°S-30°S and 60°W-100°W where the maximum increase occurs.

Fig. 3a and b show the temporal variation of IMF B_z and Dst during 07–08 September 2017. Between 00:00UT and 20:00UT on 07 September, although there are fluctuations in IMF B_z and Dst values, geomagnetic activity is quiet between these hours. However, the geomagnetic

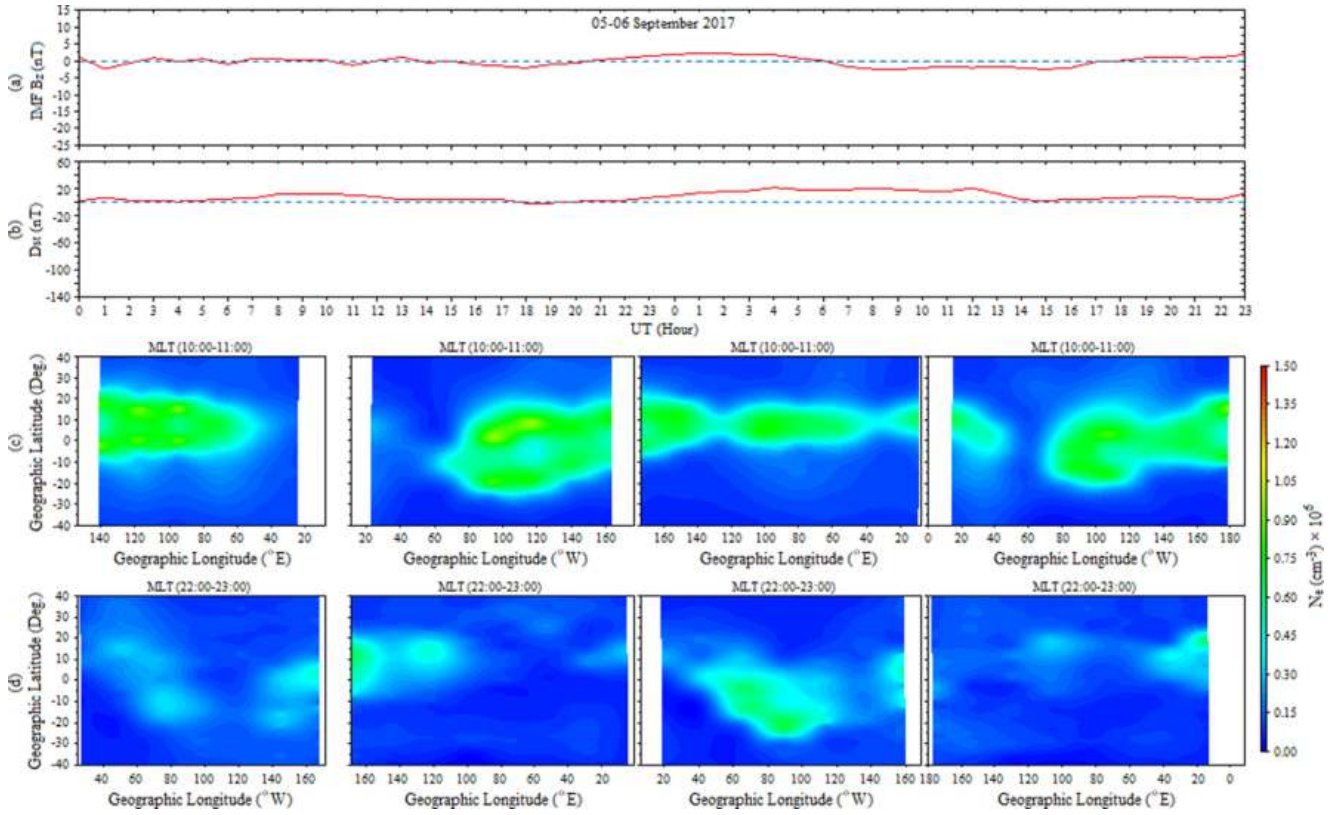

Fig. 2. During 05–06 September 2017 (a) Temporal variation of IMF B_z. (b) Temporal variation of Dst. (c) Temporal variation of plasma density (N_e) as a function of geographic latitude and longitude around noon (10:00–11:00 MLT). (d) Temporal variation of plasma density (N_e) as a function of geographic latitude and longitude around midnight (22:00–23:00 MLT).

storm can be clearly seen from the temporal changes of IMF B_z and Dst values between 21:00 UT on 07 September and 23:00 UT on 08 September. Fig. 3c and d show the temporal variation of plasma density (N_e) as a function of geographic latitude and longitude around noon (10:00–11:00 MLT) and the temporal variation of plasma density (N_e) as a function of geographic latitude and longitude around midnight (22:00–23:00 MLT) during 07–08 September 2017, respectively. For the eastern longitudes of Fig. 3c during the period between 01:00 UT and 09:00 UT on 07 September, plasma density has its highest values between latitudes 20°N and 10°S. In this region, plasma density has two peak values around 5°S and 15°N latitudes. Plasma density in latitudes outside the equatorial region exhibits a decreasing pattern with increasing latitude in both hemispheres. The distribution of plasma density during this period is very similar to the distribution of plasma density for geomagnetically quiet-time.

For the western longitudes of Fig. 3c during the period between 10:30 UT and 21:30 UT on 07 September, plasma density has maximum values during South Atlantic Anomaly region between 10°N and 25°S. The plasma density on the outside of this region generally shows a distribution with values less than 0.45×10^6 cm^{-3}. The distribution of plasma density during this period is very similar to the distribution of plasma density for geomagnetically quiet-time.

For the eastern longitudes of Fig. 3c during the period between 23:00 UT and 10:00 UT, plasma density increase gradually during the main phase of the storm with southward IMF B_z and reaches its maximum values at 01:00 UT on 08 September. The distribution of plasma density during this period has two peak values around 10°S and 20°N. The plasma density begins to decrease in association with the northward turning of the IMF B_z at 00:00 UT on September 08, continues to decrease between 00:00 UT and 04:00 UT in association with the recovery phase of geomagnetic storm, and reaches its minimum value around 04:00 UT on September 08. Then the plasma density increases again in the region between 20°S and 20°N from 05:00 UT to 08:00 UT on 08 September. For the eastern longitudes of Fig. 3c during the period between 11:30 UT and 21:00 UT on 08 September, plasma density has maximum values during region between 15°N and 20°S. The plasma density on the outside of this region generally shows a distribution with values less than 0.45×10^6 cm^{-3}. For the western longitudes of Fig. 3d during the period between 00:30 UT and 10:00 UT on 07 September, the distribution of plasma density exhibits small fluctuations during South Atlantic Anomaly region between 15°N and 20°S. Plasma density in latitudes outside this region shows a decreasing pattern with increasing latitude in both hemispheres. For the eastern longitudes of Fig. 3d during the

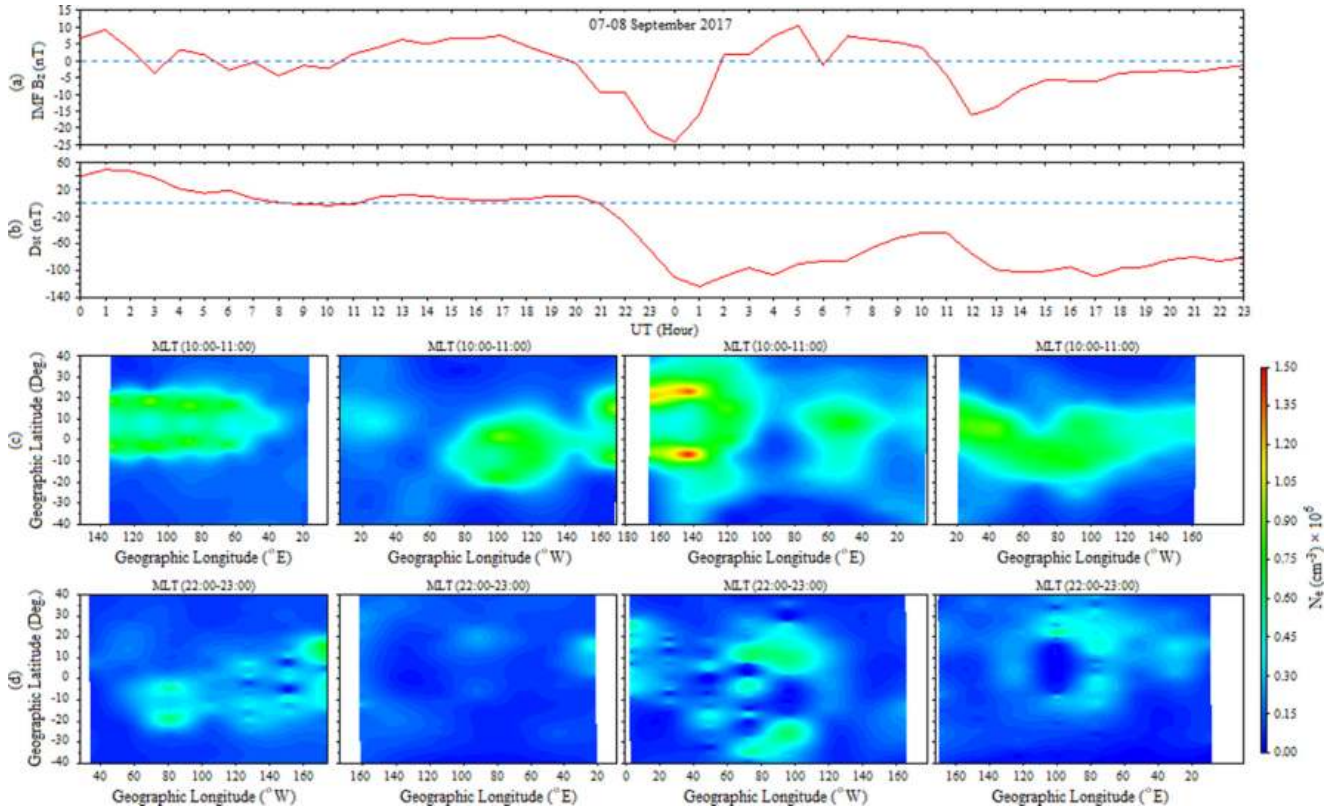

Fig. 3. During 07–08 September 2017 (a) Temporal variation of IMF B_z. (b) Temporal variation of Dst. (c) Temporal variation of plasma density (N_e) as a function of geographic latitude and longitude around noon (10:00–11:00 MLT). (d) Temporal variation of plasma density (N_e) as a function of geographic latitude and longitude around midnight (22:00–23:00 MLT).

period between 11:00 UT and 20:30 UT on 07 September, plasma density usually has values less than 0.4×10^6 cm^{-3}. For the western longitudes of Fig. 3d during the period between 22:30 UT and 09:00 UT on 07–08 September, the plasma density exhibits a fluctuating distribution with enhancements and reductions between 30°N and 40°S from 22:30 UT to 06:00 UT in association with the orientation of IMF B_z and the main and recovery phase of the geomagnetic storm. The plasma density begins to decrease in association with the southward turning of the IMF B_z at 00:00 UT on September 08 and continues to decrease between 00:00 UT and 02:00 UT in association with the main phase of geomagnetic storm. Then the plasma density begins to increase in association with the northward turning of the IMF B_z and it continues to increase between 40°S and 20°N from 02:00 UT to 06:00 UT on 08 September in association with the recovery phase of geomagnetic storm. The observed increases in plasma density during this period occurred at a maximum level around 10°N and 30°S latitudes. However, the plasma density decreases around 10°S.

The plasma density decreases after 06:00 UT and generally exhibits a distribution with values lower than 0.3×10^6 cm^{-3}. For the eastern longitudes of Fig. 3d during the period between 10:30 UT and 21:00 UT on 07 September, plasma density decreased greatly in the region between 10°N and 10°S latitudes from 15:00 UT to 16:00 UT on 08 September. However, plasma density increased in this region after 16:00 UT. In addition, plasma density increases greatly between 15:00 UT and 18:00 UT around 20°N and 15°S latitudes. For other latitudes and longitudes, the plasma density generally shows a distribution with values less than 0.3×10^6 cm^{-3}.

Fig. 4a and b show the temporal variation of IMF B_z and Dst during 09–10 September 2017, respectively. The IMF B_z have around geomagnetically quiet values from 00:00 UT on 09 September to 03:00 UT on 10 September. The IMF B_z data were not available between 03:00 UT and 23:00 UT on 10 September. Dst is about −80 nT at 00:00 UT on September 09. The Dst value gradually increases in association with the recovery phase of the geomagnetic storm and approaches the geomagnetically quiet value. Fig. 4c and d show the temporal variation of plasma density (N_e) as a function of geographic latitude and longitude around noon (10:00–11:00 MLT) and the temporal variation of plasma density (N_e) as a function of geographic latitude and longitude around midnight (22:00–23:00 MLT) during 09–10 September 2017, respectively. It can be clearly seen from Fig. 4c and d that the distributions of plasma density over eastern and western longitudes around noon and midnight during 09–10 September 2017 are very similar to the distribution of plasma density 05–06 September 2017 which is geomagnetically quiet-time. That is, the

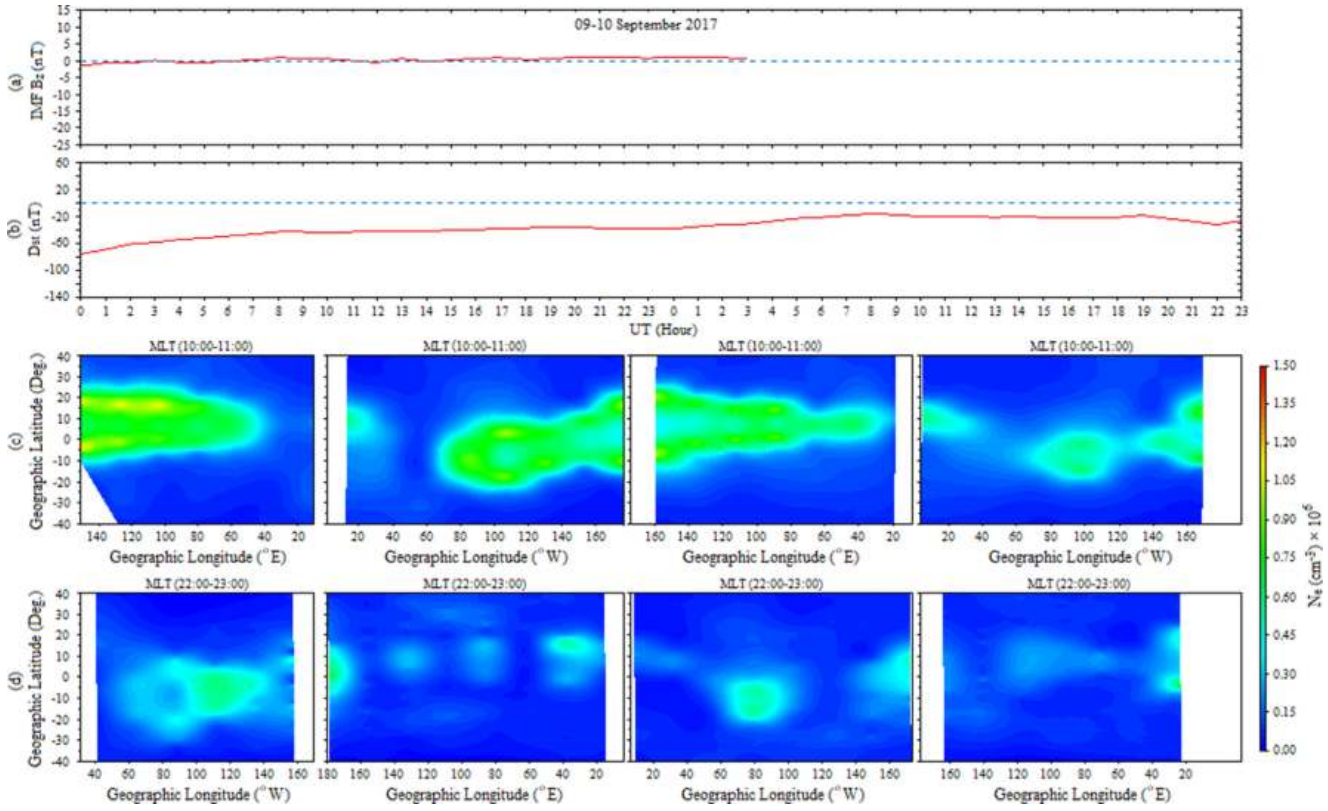

Fig. 4. During 09–10 September 2017 (a) Temporal variation of IMF B_z. (b) Temporal variation of Dst. (c) Temporal variation of plasma density (N_e) as a function of geographic latitude and longitude around noon (10:00–11:00 MLT). (d) Temporal variation of plasma density (N_e) as a function of geographic latitude and longitude around midnight (22:00–23:00 MLT).

plasma density values after the geomagnetic storm tend to approach the plasma density data in the geomagnetically quiet period.

The observations clearly indicate that the interplanetary electric field (IEF) penetrates to ionosphere on the low and equatorial latitude regions and its effects on the ionospheric plasma density vary in association with orientation of IMF B_z, different phases of geomagnetic storm and local time. The plasma density enhancements and reductions detected by the Swarm satellite during 07–08 September geomagnetic storm are caused by the prompt penetration electric fields (PPEFs).

The results are in agreement with the results from studies that investigate the effects of the interplanetary electric field (IEF) on the low latitude ionosphere (Chao and John, 2005; Huba et al., 2005; Chao et al., 2007; Libo et al., 2008; Takashi et al., 2008; Tsurutani et al., 2008; Dashora et al., 2009; Veenadhari et al., 2010; Guo et al., 2011; Yosuke and Michael, 2015; Yong et al., 2015; Astafyeva et al., 2018; Erdinç, 2019a, 2019b; Veenadhari et al., 2019; Kumiko et al., 2020; Younas et al., 2020; Arowolo et al., 2021). These studies have shown that if the interplanetary electric field (IEF) during geomagnetic storms penetrates to the low-latitude ionosphere it cause significant redistribution of the ionospheric electron density. During the main phase of the geomagnetic storm with southward IMF B_z, the eastward PPEFs on the dayside drive the ionospheric plasma to higher altitudes owing to E × B drift, and decrease in recombination rate for higher altitudes cause increases in the plasma density, while the westward PPEFs on the nightside drive the ionospheric plasma to lower altitudes owing to E × B drift, and increase in recombination rate for lower altitudes cause decreases in the plasma density. During the recovery phase of the geomagnetic storm with northward IMF B_z, the westward PPEFs on the dayside drive the ionospheric plasma to lower altitudes owing to E × B drift, and increase in recombination rate for lower altitudes cause decreases in the plasma density, while the eastward PPEFs on the nightside drive the ionospheric plasma to higher altitudes owing to E × B drift, and decrease in recombination rate for higher altitudes cause increases in the plasma density.

4. Conclusions

In this paper, the effect of prompt penetration electric fields (PPEFs) on the plasma density obtained from the SWARM satellite for low latitudes during the 07–08 September 2017 geomagnetic storm was examined. The main results from the study are as follows:

- During the main phase of geomagnetic storm with southward IMF Bz, plasma density increased around noon (10:00–11:00 MLT), while plasma density

decreased around midnight (22:00–23:00 MLT). The mechanisms that cause to the enhancements and reductions in the plasma density around noon and midnight during this period include the undershielding effect.
- During the recovery phase of geomagnetic storm with northward IMF B_z, plasma density decreased around noon (10:00–11:00 MLT), while plasma density increased around midnight (22:00–23:00 MLT). The mechanisms that cause to the reductions and enhancements in the plasma density around noon and midnight during this period include the overshielding effect.
- The plasma density around both noon and midnight after the geomagnetic storm shows a distribution very similar to the distribution of plasma density during the geomagnetically quiet period.

The results show that the changes in plasma density around noon side and midnight side during the main phase and recovery phase of geomagnetic storm is associated with the PPEFs. During the main phase of the geomagnetic storm with southward IMF B_z, the plasma density around the noon side increased due to the eastward PPEFs while the plasma density around midnight side decreased due to the westward PPEFs.

Declaration of Competing Interest

The author declares that he has no known competing financial interests or personal relationships that could have appeared to influence the work reported in this paper.

Acknowledgment

The author thanks VirES for Swarm (https://vires.services/) for access to the plasma density data. The IMF B_z and Dst data were provided by the Omniweb (https://omniweb.gsfc.nasa.gov/form/dx1.html).

References

Akala, A. O., Oyeyemi, E. O., Amaechi, P. O., Radicella, S. M., Nava, B., Amory-Mazaudier, C., 2020. Longitudinal responses of the equatorial/low latitude ionosphere over the oceanic regions to geomagnetic storms of May and September, 2017. J. Geophys. Res.: Space Physics, 125(8), https://doi.org/10.1029/2020JA027963.

Arowolo, O.A., Akala, A.O., Oyeyemi, E.O., 2021. Interplanetary origins of some intense geomagnetic storms during solar cycle 24 and the responses of african equatorial/low-latitude ionosphere to them. J. Geophys. Res.: Space Physics 126 (2). https://doi.org/10.1029/2020JA027929.

Astafyeva, E., Zakharenkova, I., Hozumi, K., Alken, P., Coïsson, P., Hairston, M.R., Coley, W.R., 2018. Study of the equatorial and low-latitude electrodynamic and ionospheric disturbances during the 22–23 June 2015 geomagnetic storm using ground-based and spaceborne techniques. J. Geophys. Res.: Space Phys. 123 (3), 2424–2440. https://doi.org/10.1002/2017JA024981.

Atsuhiro, N., 1968. Coherence of geomagnetic DP 2 fluctuations with interplanetary magnetic variations. J. Geophys. Res. 73 (17), 5549–5559. https://doi.org/10.1029/JA073i017p05549.

Chao, S.H., John, C.F., 2005. Long-duration penetration of the interplanetary electric field to the low-latitude ionosphere during the main phase of magnetic storms. J. Geophys. Res. 110, A11309. https://doi.org/10.1029/2005JA011202.

Chao, S.H., Stanislav, S., Jorge, L.C., Naomi, M., Michael, C.K., 2007. Penetration electric fields: Efficiency and characteristic time scale. J. Atmos. Sol. Terr. Phys. 69 (10–11), 1135–1146. https://doi.org/10.1016/j.jastp.2006.08.016.

Danilov, A.D., Laštovička, J., 2001. Effects of geomagnetic storms on the ionosphere and atmosphere. Int. J. Geomagn. Aeron. 2 (3), 209–224.

Dashora, N., Sharma, S., Dabas, R.S., Alex, S., Pandey, R., 2009. Large enhancements in low latitude total electron content during 15 May 2005 geomagnetic storm in Indian zone. Ann. Geophys. 27 (5), 1803–1820. https://doi.org/10.5194/angeo-27-1803-2009.

Erdinç, T., 2019a. The effect of different phases of severe geomagnetic storms on the low latitude ionospheric critical frequencies. Adv. Space Res. 64 (11), 2280–2289. https://doi.org/10.1016/j.asr.2019.08.026.

Erdinç, T., 2019b. The north and south symmetry of the ionospheric storms at magnetic conjugate points for low latitudes during the March 1976 severe geomagnetic storms and the relation between daily changes of the storms with geomagnetic activity indices. Adv. Space Res. 63 (12), 3965–3977. https://doi.org/10.1016/j.asr.2019.02.029.

Gilda de Lourdes, G., 2021. Spread-F occurrence during geomagnetic storms near the southern crest of the EIA in Argentina. Adv. Space Res. 67 (3), 1058–1084. https://doi.org/10.1016/j.asr.2020.10.051.

Guo, J., Feng, X., Zuo, P., Zhang, J., Wei, Y., Zong, Q., 2011. Interplanetary drivers of ionospheric prompt penetration electric fields. Journal of. J. Atmos. Sol. Terr. Phys. 73 (1), 130–136. https://doi.org/10.1016/j.jastp.2010.01.010.

Huba, J.D., Joyce, G., Sazykin, S., Wolf, R., Spiro, R., 2005. Simulation study of penetration electric field effects on the low-to mid-latitude ionosphere. Geophys. Res. Lett. 32, L23101. https://doi.org/10.1029/2005GL024162.

Jaggi, R.K., Wolf, R.A., 1973. Self-consistent calculation of the motion of a sheet of ions in the magnetosphere. J. Geophys. Res. 78 (16), 2852–2866. https://doi.org/10.1029/JA078i016p02852.

Kivelson, M.G., Russell, C.T., 1995. Introduction to Space Physics. Cambridge University Press, Cambridge, UK, pp. 180–250.

Kumiko, K.H., Takashi, K., Ichiro, T., Keisuke, H., Jaroslav, C., Dalia, B., Masahito, N., Kiyokazu, K., 2020. Penetration electric fields observed at middle and low latitudes during the 22 June 2015 geomagnetic storm. Earth, Planets and Space. 72 (71). https://doi.org/10.1186/s40623-020-01196-0.

Libo, L., Weixing, W., Man-Lian, Z., Biqiang, Z., 2008. Case study on total electron content enhancements at low latitudes during low geomagnetic activities before the storms. Ann. Geophys. 26 (4), 893–903. https://doi.org/10.5194/angeo-26-893-2008.

Prölss, G.W., 2004. Physics of the Earth's Space Environment. Springer-Verlag Press, Berlin-Heidelberg-New York, pp. 77–444.

Schunk, R. W., Nagy, A. F., Ionospheres-physics, Plasma Physics, and Chemistry Cambridge University Press, UK, pp. 366-432, 2000.

Takashi, K., Kumiko, K. Kenro, H., N., 2008. Penetration of magnetospheric electric fields to the equator during a geomagnetic storm. J. Geophys. Res. 113, A06214, https://doi.org/10.1029/2007JA012628.

Tascione, T.F., 2010. Introduction to the Space Environment. Krieger Publishing Company Malabar, Florida, pp. 79–112.

Tsurutani, B.T., Verkhoglyadova, O.P., Mannucci, A.J., Saito, A., Araki, T., Yumoto, K., Tsuda, T., Abdu, M.A., Sobral, J.H.A., Gonzalez, W. D., McCreadie, H., Lakhina, G.S., Vasyliunas, V.M., 2008. Prompt penetration electric fields (PPEFs) and their ionospheric effects during the great magnetic storm of 30–31 October 2003. J. Geophys. Res. 113, A05311. https://doi.org/10.1029/2007JA012879.

Veenadhari, B., Alex, S., Kikuchi, T., Shinbori, A., Singh, R., Chandrasekhar, E., 2010. Penetration of magnetospheric electric fields to the equator and their effects on the low-latitude ionosphere during intense geomagnetic storms. J. Geophys. Res. 115, A03305. https://doi.org/10.1029/2009JA014562.

Veenadhari, B., Kikuchi, T., Kumar, S., Tulasi, R.S., Chakrabarty, D., Ebihara, Y., Reeves, G.D., 2019. Signatures of substorm related overshielding electric field at equatorial latitudes under steady southward IMF Bz during main phase of magnetic storm. Adv. Space Res. 64 (10), 1975–1988. https://doi.org/10.1016/j.asr.2019.04.001.

Yong, W., Biqiang, Z., Guozhu, L., Weixing, W., 2015. Electric field penetration into Earth's ionosphere: a brief review for 2000–2013. Sci. Bull. 60 (8), 748–761. https://doi.org/10.1007/s11434-015-0749-4.

Yosuke, Y., Michael, J.K., 2015. The equatorial electrojet during geomagnetic storms and substorms. J. Geophys. Res.: Space. Physics 120 (3), 2276–2287. https://doi.org/10.1002/2014JA020773.

Younas, W., Amory-Mazaudier, C., Khan, M., Fleury, R., 2020. Ionospheric and magnetic signatures of a space weather event 25–29 August 2018: CME and HSSWs. J. Geophys. Res.: Space. Physics 125 (8). https://doi.org/10.1029/2020JA027981.